doi: 10.5028/jatm.v10.925 ORIGINAL PAPER

A Comparative Study of the Heat Input During Laser Welding of Aeronautical Aluminum Alloy AA6013-T4

Bruno Nazário Coelho[1], Milton Sergio Fernandes de Lima[1], Sheila Medeiros de Carvalho[1], Adilson Rodrigues da Costa[1]

Coelho BN http://orcid.org/0000-0002-2809-7778
Lima M http://orcid.org/0000-0001-5540-8802
Carvalho S http://orcid.org/0000-0003-4583-9451
Costa AR http://orcid.org/0000-0002-3123-0701

How to cite

Coelho BN; Lima MSF; Carvalho SM; Costa AR (2018) A Comparative Study of the Heat Input During Laser Welding of Aeronautical Aluminus Alloy AA6013-T4. J Aerosp Technol Manag, 10: e2918. doi: 10.5028/jatm.v10.925.

ABSTRACT: The heat input is the amount of energy supplied per unit length of the welded workpiece. In this study, the effect of two different heat inputs in laser beam welding of a high strength aluminum alloy AA6013-T4 was evaluated from macrostructural and microstructural points of view. The experiments were performed using a continuous wave 2 kW Yb-fiber laser with 100 µm spot size on the upper surface of the workpiece. Keeping the heat input at a given level, 13 or 30 J/mm, the laser power was changed from 650 W to 2 kW and the welding speed from 33 to 150 mm/s. In the condition of higher heat input 30 J/mm it was possible to obtain both cutting and welding processes. For 13 J/mm, welding processes were obtained in conduction and keyhole modes. The equiaxed grain fraction changed with changing speed for the same heat input. The laser processing induced a decrease in the hardness of the weld bead of about 25% due to the solubilization of the precipitates. The estimated absorptivities of the laser beam in the liquid aluminum changed largely with experimental conditions, from 4.6% to 10.5%, being the most significant source of error in measuring the real amount of energy absorbed in the process. For the same heat input the macrostructure of the welded surfaces, i.e., humps and dropouts, changed as well. All these facts indicate that the heat input is not a convenient method to parameterize the laser beam welding parameters aiming the same weld features.

KEYWORDS: Laser processing, Heat input, Laser beam welding, Aluminum alloy 6013-T4.

INTRODUCTION

Laser materials processing has received special attention from the automotive and aerospace industries in recent years, which greatly contributes to the encouragement of research and development of new technologies. Several areas of knowledge have taken advantage of this development, from medicine to electronics, but the main stakeholders are the former, which are seeking higher manufacturing speeds and improving the final product quality. The welding fundamentals and their implications in aeronautical components have been investigated with high expectations (Mendez and Eagar 2001). The integration of laser technology with the easiness of automation and robotization of the industrial systems contributes greatly to cost reduction, as required by the current market. At the same time, this advance requires an increasingly deep and detailed understanding of the transformations that occur during processing.

1.Departamento de Ciência e Tecnologia Aeroespacial – Instituto de Estudos Avançados – Divisão de Fotônica – São José dos Campos/SP – Brazil.
Correspondence author: Milton Lima | Departamento de Ciência e Tecnologia Aeroespacial – Instituto de Estudos Avançados – Divisão de Fotônica | Trevo Cel. Amarante km1 | CEP: 12.228-001 – São José dos Campos/SP – Brazil | E-mail: msflima@gmail.com
Received: Jun. 20, 2017 | **Accepted:** Aug. 9, 2017
Section Editor: Mariana Fraga

High-strength aluminum alloys, like the AA6013, have been gaining space and reliability mainly in the aerospace industry, in the joining of the stringers to the fuselage. Their characteristics and metallurgical properties allow great advantages and a high quality in their laser process. This is only possible due to the development, in recent years, of high power lasers with smaller wavelengths, which provides a radiation capable of interacting with the aluminum, being only reflected part of it. The most common problems, which were also found in this study, were cracking and liquation, depending on the set of operational parameters, besides the dissolution of precipitates.

The aluminum alloy 6013 is a high strength alloy with a good combination of mechanical properties, corrosion resistance, weldability and formability. The 6013 with T4 temper exhibits better bend capability and lower springback than high strength steels. It is not susceptible to hot cracking during welding compared to some 7XXX series alloys. The 6013 is a weldable aluminum alloy specifically developed for high strength applications.

The physical properties of AA6013 welded by Nd:YAG laser were evaluated by Leigh *et al.* (2002) with the process parameters of 4.3 kW and 6.2 m/min. A very detailed analysis was discussed regarding to the hardness reduction on the fused zone, transition from columnar to equiaxed grains, growth of dendritic structures intergranular solidification cracks, liquation and porosity.

A numerical modeling and experimental analysis were developed by Wang *et al.* (2015) to investigate the solidification cracking behavior during laser welding of AA6013. The transient evolution and distribution of mechanical strain were analyzed and the results exhibited that the solidification cracking started near the molten line and then propagated along the centerline of the weld.

Passini *et al.* (2011) performed laser welds of 1.6 mm thick AA6013 using a 2 kW Yb:fiber laser. There were obtained good and poor welds, and inspected by pulse/echo ultrasonic phased-array technique, where it was identified the presence of grouped porosity.

Braun (2005) performed thermal treatments after the laser beam welds of AA6013, obtaining improved mechanical properties and stress relief of the joint. Siqueira *et al.* (2015) have also investigated thermal treatments on AA6013, reaching better results with lower temperatures (190 °C).

Higashi and Lima (2012) investigated laser beam welding in aluminum alloys, where two main defects were observed: porosity, and hot cracking. Autogenous welding using a 2 kW Yb:fiber laser was performed, and the best results were obtained using two runs (both sides) with filler, 1200 W and a speed of 2 m/min.

Tu and Paleocrassas (2010) investigated the instability in the low speed laser welding of aluminum alloys with fiber lasers. The results showed that lower speeds form high aspect ratio welds. The general aspects regarding the laser welding of structural aluminum were also investigated by Quintino *et al.* (2012).

The high thermal diffusivity and optical reflectivity to CO_2 laser radiation require high laser intensities to ensure coupling and to form the keyhole. Excessive vaporization of alloying elements and porosity were common problems found by Sonti (1988) in laser welding of aluminum alloys.

Huntington and Eagar (1982) studied the laser power absorption on pure aluminum and aluminum alloy. The results indicate that the fraction of absorbed power increases with the keyhole formation. Increased power absorption does not occur at the beginning of the melt but rather with the start of keyhole formation.

The laser processing of metallic alloys has been extensively studied (Steen and Mazumder 2010). Researches have evaluated the fusion zone (FZ) and Heat Affected Zone (HAZ) microstructures, as well as the macroscopic behavior such as tensile strength, fatigue life, and corrosion. The laser parameters have been extensively studied for Laser Beam Welding, Laser Cutting, Cladding, Ablation, and Additive Manufacturing. The operational parameters were also evaluated in the Laser Beam Forming (LBF) process, which uses smaller speeds and bigger spot size. It is important to point out that each of these processes requires a different amount of available energy, and each process has its own absorptivity and efficiency of this heat input.

In this study, the authors are interested in better understanding the effects of the same heat input, provided by different sets of parameters, on the AA6013 weldability. This study is performed comparatively between the observed experimental results and the expected results by means of a thermal simulation.

In many cases, the laser processing can be simplified in the theory of moving sources of heat in metals, given by Rosenthal (1946). This theory still makes some assumptions like constant speed and heat input, besides considering the physical characteristics

of the metal independent of the temperature. Notwithstanding the increase in temperature causes an increase in conductivity and diffusivity of the sample, thus affecting the shape and size of the isotherms.

Figure 1 shows the temperature gradient and the influence of the speed in the shape of molten pool for two situations: higher speed (a), where the isotherms are more flattened and it occurs the columnar grains encounter, which can cause greater fragility in the central region; and lower speed (b), with a more elliptical shape of isotherms and molten pool, and reduced formation of columnar grains. Speed control can provide greater equiaxed grain formation in the central region of the molten pool, which increases the resistance. Therefore, the thermal gradient increases proportionally with speed. The temperature gradient in front of the heat source is much higher than that behind it. The curve n-n presents the peak temperatures at a same time, and it can be observed that the points along the y-axis reach lower peak temperatures. The curve n-n bends backwards and its shape depends on the transverse speed and the thermal diffusivity (Kannatey-Asibu Jr. 2009).

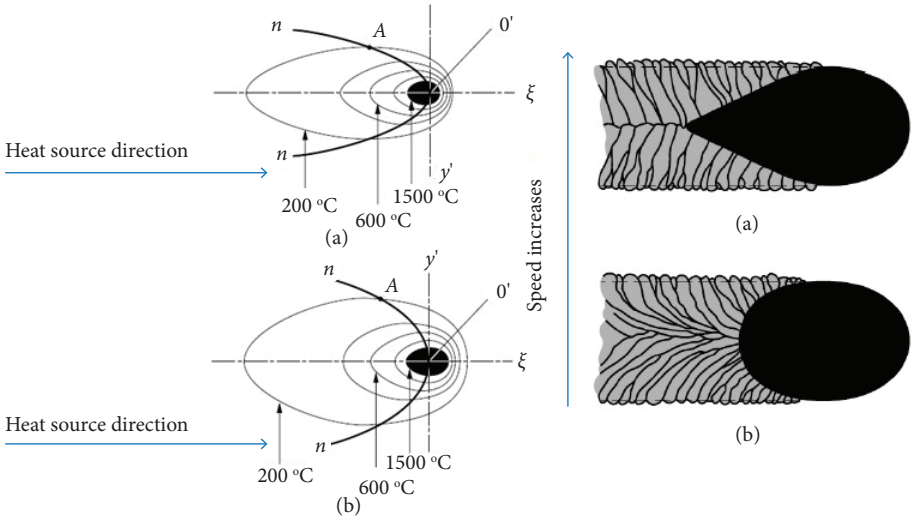

Figure 1. Thermal gradient and shape of the molten pool in different speeds (a) and (b) (Kannatey-Asibu Jr. 2009).

The amount of energy absorbed by the workpiece depends on the wavelength (λ) of the laser radiation, the temperature, and the properties of the material ($I_x = I_0 e^{-ax}$). Lima (2016) presents very detailed analyzes, regarding the absorptivity, temperature evolution, optical penetration, phase transformations during laser processing, the effect of the interaction time, and also a state-of-the-art contribution about the thermal gradient and cooling rate. Correlations between operational parameters such as laser beam power and speed, and their influence on the depth of the molten zone and in the width of HAZ (Ion 2005), have been extensively studied.

The heating of a given material subjected to a laser beam depends on the nature of the material, on the characteristics of the beam, and how the radiation is coupled with matter (Lima 2016). The traditional heat input model is the ratio between the power and speed of the laser beam, but there are a number of other factors that directly affect the amount of energy used by the material, such as absorptivity, spot size, TEM modes, M^2, BPP, focal distance, surface finishing, among others. The beam intensity or power density can be calculated by $I = P/\pi r^2$ W cm^{-2}. The amount of energy absorbed directly influences the cooling rate, HAZ, the microstructure, and the mechanical properties. With a same heat input, which corresponds to a same amount of energy supplied, the interaction time is the one responsible for the difference between a keyhole welding and a simple material heating.

Green's functions give analytical solutions for the temperature field around a moving heat source. A thermal shock wave is generated when the processing speed is equal to or faster than the thermal wave from the thermal diffusivity of the material. In the same way, as the Mach number in supersonic regimes, a shock wave angle can be calculated by $\sin^{-1}(1/M)$ for $M > 1$ (Tzou 1989). The M number can be related to the minimum interaction time of the heat source and the workpiece.

The aim of this study is to study the effects of heat input on laser processing through different sets of operating parameters. The experiments were performed with an Yb-fiber laser on sheets of AA6013-T4. Although the heat input parameter, as a qualifying value for the welding process, has been subject of many works, it was proposed the effect of the absorptivity as an additional parameter to be considered in the heat transfer during laser and matter interactions.

ABSORPTION OF LASER RADIATION

Keyhole welding is possible once the heat source is approximately a line inside the solid and the lateral conduction of heat is sufficient to produce a given weld width. For simplicity, let us consider that the heat will be absorbed in the material to produce a given amount of liquid aluminum with negligible thermal transfer of the solid material. Since the heat-affected zone usually rarely exceeds few micrometers, this assumption could be considered quite correct.

Considering the simplest model, as depicted in Fig. 2, two plates A and B are welded together forming the resolidified material called C. The weld has three characteristic dimensions: width (w), thickness (t), and length (l), which the product is the resolidified volume. The amount of energy required to heat up until melted such a volume is given by the well-known Eq. 1:

$$Q = m.Cp.\Delta T + mL \quad (1)$$

where: Q is the amount of energy entering the system; m is the mass of the weld; Cp is the specific heat; ΔT is the temperature variation between ambient and melting point; and L is the latent heat of fusion.

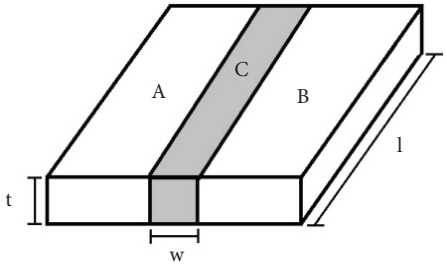

Figure 2. A model for laser welding.

The total amount of energy entering the system is the effective laser power multiplied by an interaction time (ti) linked to the welding speed. One dimension (l) is also linked to the welding speed as V = l/ti. Therefore, Eq. 1 could be easily rewritten as presented in Eq. 2:

$$\beta.P = w.t.V.\rho.(Cp\Delta T+L) \quad (2)$$

where: b is the laser-matter absorptivity, i.e., the amount of the power effectively absorbed in the workpiece; P is the laser power; V is the weld speed; and r is the solid density. The solidification interval DT is the difference between the solidus and liquidus for the present alloy.

Considering both absorptivity and weld bead dimensions as constants, it is easy to see that Eq. 2 gives a constant bP/V ratio for a given welding process, being the P/V ratio called therewith as the heat input HI. Using now the current values, such as r = 2.7 g/cm^3, Cp = 0.9 J/g.K (MakeItFrom 2017), L = 321 J/g (Enginneering Toolbox 2003) and DT = 89.19 K, then (Eq. 3):

$$HI = 1.0834.w.t.\beta^{-1} \text{ J/mm} \quad (3)$$

The weld bead dimensions w and t depend on the experimental values and, until now, β is still an unknown variable. The proposed method does not include the improved energy absorption as a consequence of keyhole.

MATERIAL AND METHODS

The Aluminum Alloy 6013-T4, AA6013 for short, was chosen for this study due to its broad use in the aerospace industry. It was used sheets of 100 mm × 50 mm, with thickness of 1.25 mm. The current chemical composition of this alloy is shown in Table 1. The designation T4 is related to the tempering thermal treatment, meaning heat treated solution annealing followed by natural aging.

Table 1. Chemical composition of AA6013-T4 (%).

Mg	Si	Cu	Mn	Fe	Others	Al
0.94 ± 0.05	0.62 ± 0.02	0.82 ± 0.02	0.27 ± 0.04	0.20 ± 0.01	0.06 ± 0.01	Balance

A 2 kW continuous wave fiber laser wave was manufactured by IPG Co under designation YLR-2000. Figure 3 shows the diagram of the workstation. The focal length was 160 mm with a minimum spot diameter of 100 μm, the beam quality was $M^2 = 12$ and the wavelength was 1080 nm. The spot of the laser beam is due to the diameter of the optical fiber used in the experiments. During processing, pure helium gas at 8l/min flow rate was used to protect the Al surface against oxidation. The shielding gas was delivered directly over the irradiated area through a rounded nozzle. A nitrogen laminar flow was also used to protect the lenses against fumes and drops. The movement of the samples was performed by a CNC table at constant speed from 1 mm/s to 160 mm/s. The Z-axis is also computer controlled with a 1 μm step resolution and it is used to adjust the focal distance.

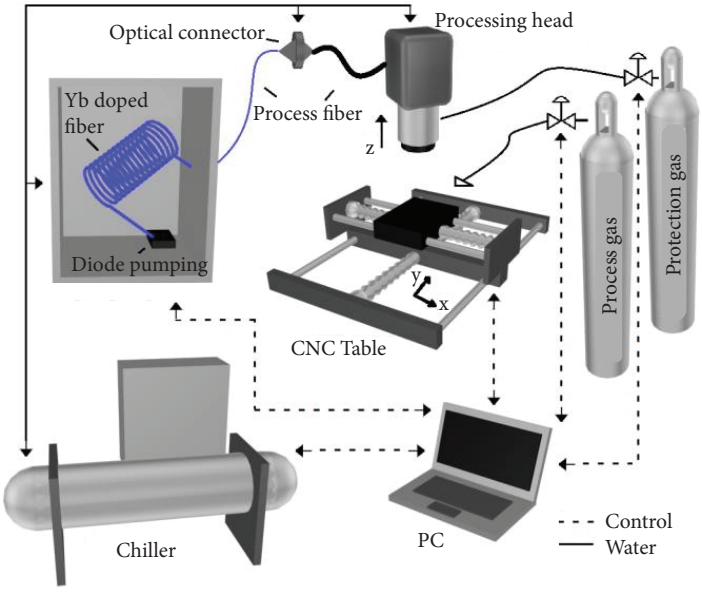

Figure 3. A diagram of the laser workstation.

Table 2 shows the experimental conditions, in which two groups of HI values, 13 J/mm and 30 J/mm were established in order to determine the amount of energy provided for the material during the process. The laser power (P) and the speed (V) of the beam were established so that they provide a fixed heat input. The values of P and V reflected those levels proved to be efficient to reduce

pores and cracks in previous laboratory experiments. The interaction time (t_i) represents the time during which an infinitesimal point in the weld line was exposed to the laser beam. In all the experiments, the focal distance was adjusted to provide a spot size of 100 μm in the upper surface of the sheet.

Table 2. Experimental parameters.

Sample	Heat Input, HI (J/mm)	Laser Power, P (W)	Speed, V (mm/s)	Interaction time, t_i (ms)
A	30	2000	67	1.49
B	30	1500	50	2.00
C	30	1000	33	3.03
D	13	2000	150	0.67
E	13	1300	100	1.00
F	13	650	50	2.00

The beam speed and the interaction time are factors that determine the heating and solidification rates, directly affecting the thermal gradient, and indirectly, the occurrence of weld defects. For a long interaction time, the temperature gradient is lower, which provides a convenient preheating of the material ahead of the laser beam. The minimum interaction time can be estimated by $t_{i\_min} = D_S^2/\alpha$, where D_S is the spot size and α is the thermal diffusivity (Riva *et al.* 2015). Considering the 6000 aluminum alloy thermal diffusivity (α) of 6.4×10^{-5} m²/s, it can be estimated at minimum interaction time $t_{i\_min} = 0.15$ ms. With the aim of achieving the preheating effect, the beam speed must be proportionally less than the time required for thermal diffusion to occur in the material. Therefore, in all experiments a preheating was provided on the melt front, but this preheating decreases with an increasing speed.

The samples were cut in three different cross sections, ground and polished automatically, and subsequently etched with a Keller solution during 30 s, for the optical microscopy. Samples with Barker's reagent were also prepared, which provides colored micrographs according to the crystallographic directions of the grains. The volume fraction of equiaxed grains was obtained using ImageJ software and available literature about columnar-equiaxed growth (Kurz *et al.* 2001). Hardness measurement was performed with a Vickers microhardness tester with 100 gf load during of 10 s. In order to obtain more detailed information about the general macroscopic aspects of weld beads, analysis of the samples D and E were made with a Confocal Microscope (Alicona Infinite Focus).

RESULTS AND DISCUSSION

HEAT INPUT

Several cross sections were made in each one of the six Bead-on-Plate experiments and some of them can be observed in Fig. 4, in which the left column presents the resulting macrographies of the samples with HI of 30 J/mm, and the right column belongs to the samples with HI of 13 J/mm. Excessive laser intensity was verified when HI was 30 J/mm, since the liquid flowed to the weld root and, in two cases, B and C, the sections were cut off. For the samples at HI 13 J/mm, the weld is more regular for the cases D and E, and insufficient heat input was observed in the F case. Therefore, a given HI input result in very different welds dimensions and thus the bead and related absorptivity must be considered for each case, as proposed in Eq. 3. Table 3 presents the experimental measurements of the width of the weld in the middle (w_m), the width of the weld at the surface (w_s), the depth of the weld (t), and the molten area (w.t), as proposed in Eq. 3. Considering this equation, the measured absorptivities for each experiment (b) are presented in the last column. The plot presented in Fig. 5 shows an approximately linear increase of the absorptivity from condition A to E, followed by a drop from condition E to F. This drop in β value has been associated with a change in the heat transfer condition from condition E to F due to the change from the keyhole to conduction welding (Kaplan 1994).

Figure 6 shows the ANSYS model of a Gaussian moving heat source adjusted according to the laser conditions, whose spot (transversal mode TEM_{00}) is represented by a Gaussian, and spot size of 100 μm. In this simulation, the propagation of heat in all directions of the solid can be better understood. The left column shows the thermal gradient at the top, the middle column shows the cross section, and the right column shows the longitudinal section of the samples D, E, and F, respectively on each line.

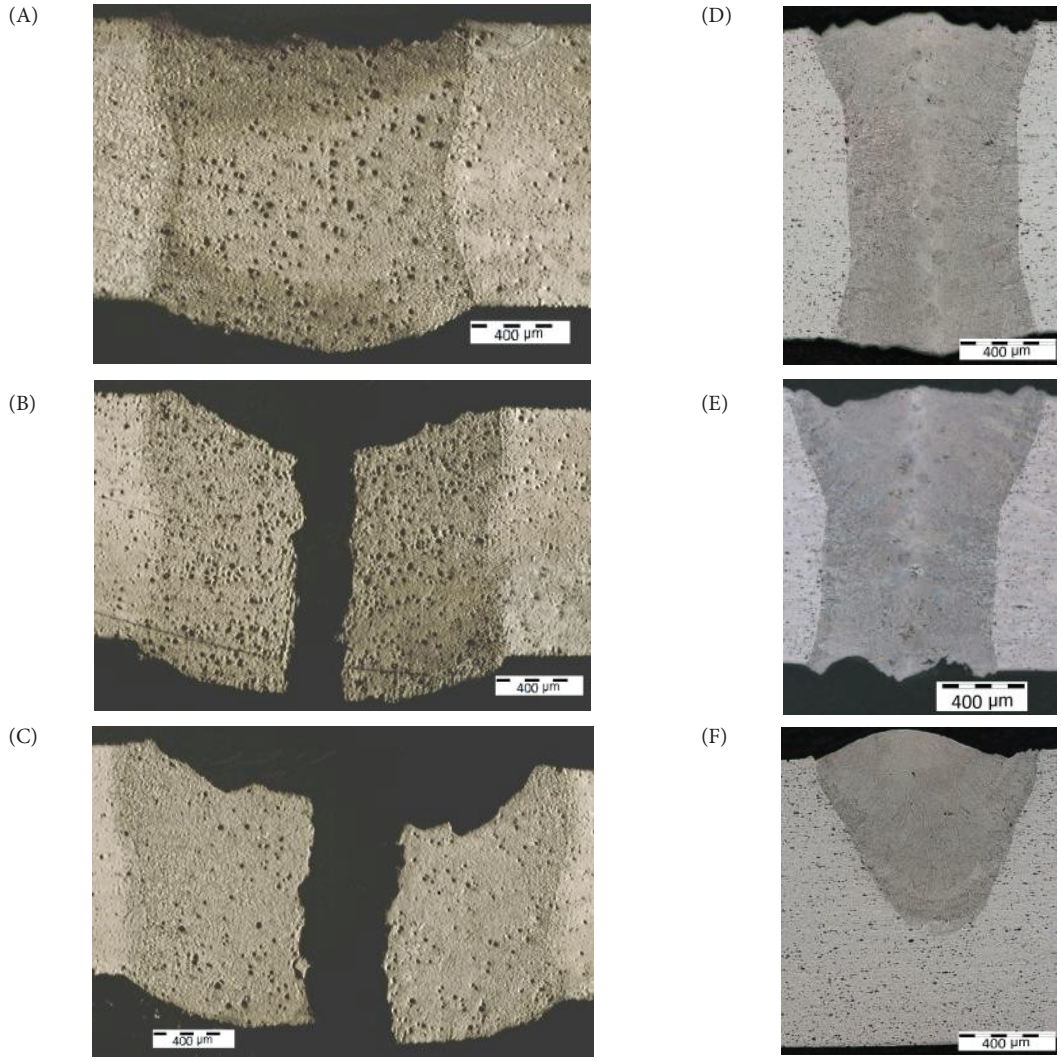

Figure 4. Optical micrography of the cross sections for samples (A), (B), (C), (D), (E), and (F), whose conditions are listed in Table 2.

Table 3. Depth and width measurements.

Sample	HI (J/mm)	w_m (mm)	w_s (mm)	t (mm)	w.t (mm²)	b (%)
A	30	1.21	1.495	1.25	1.775	6.4
B	30	1.375	1.67	1.25	2.010	7.3
C	30	1.805	1.925	1.25	2.275	8.2
D	13	0.78	1.065	1.25	1.095	9.1
E	13	0.91	1.255	1.25	1.265	10.5
F	13	0.66	0.97	0.795	0.555	4.6

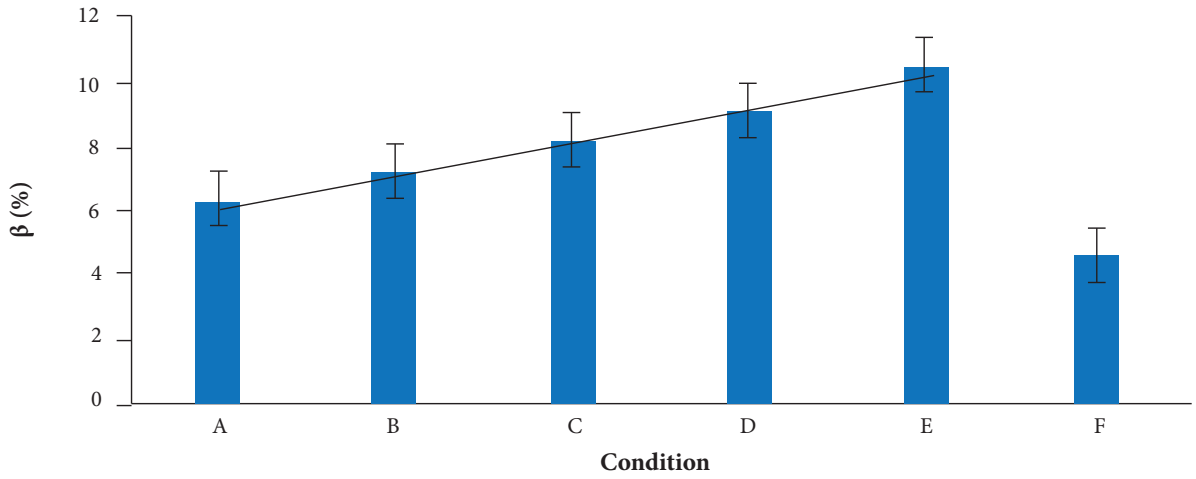

Figure 5. Laser absorptivity as a function of the experimental conditions.

In the left and right columns, a difference of the heat front in the forward direction of the laser beam can be observed. The D, E, and F experiments were performed with exactly the same Heat Input (13 J/mm), but there is a large difference in the thermal gradient, which at lower speeds provides a longer time for the heat propagation, which generates a preheating of the base material, shortly before being reached by the laser beam. This temperature difference directly affects the properties of the material, such as the absorptivity itself, which increases according to the temperature. Therefore, maintaining the same heat input, but with lower speeds, it is possible to obtain a lower absorption of the laser beam by the material, but at the same time, the proportional reduction of the power can preclude the formation of the keyhole.

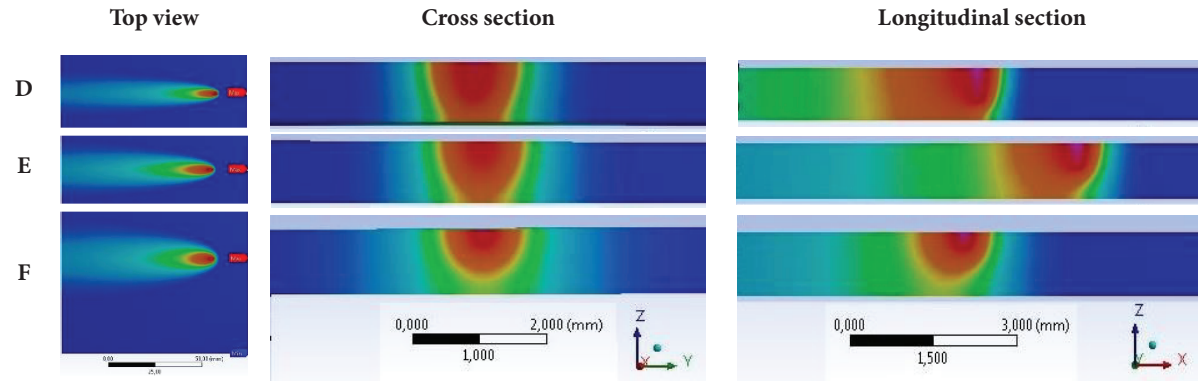

Figure 6. Thermal gradient simulation (top view, cross section, longitudinal section) for samples (D), (E), and (F).

Due to the fact that the heat does not propagate instantaneously in metals, the maximum temperature at certain points of the transversal section occurs with a delay in relation to the heat source. The factors that determine this discrepancy are speed and thermal diffusivity of the material. According to the current simulations, the thermal gradient at the weld centerline, and between 600 and 660 °C, were 204.78, 257.51, and 483.87 °C/mm for D, E, and F, respectively. The thermal gradient had been estimated using the vector component of each isotherm around 630 °C in all computations.

MICROSTRUCTURE AND HARDNESS

Phase growth is similar in all cases and condition E could be used as a representative case. Figure 7 shows the sample E cross section, focusing on the fusion zone (a) and also in the interface between the base metal and the fusion zone (b). In the figure, it

can be observed a small HAZ, characterized by liquation (L). It can also be observed the epitaxial (E) solidification from the base metal grains toward the molten zone on the right side of Fig. 7b. The microstructure of solidification of the molten zone changes as it moves from the fusion boundary onto the centerline.

The welds presented both columnar and equiaxed grains. Columnar grains grown epitaxially from the fusion line and equiaxed grains were formed in the liquid phase ahead of the solidification front and due to the constitutional undercooling (Kurz and Fisher 1989). The percentage of equiaxed grains were 13%, 21%, and 24% for speeds 50, 100, and 150 mm/s, respectively. These results corroborate the most accepted theory of equiaxed/columnar growth (Wang and Beckermann 1994; Martorano *et al.* 2003), where equiaxed grains in an undercooled liquid are more probable in high growth speeds (Table 2 and low thermal gradients in Heat Input section).

The main thermal factors that determine the microstructure are temperature distribution, peak temperatures and cooling rates. Increasing the heat input does not change the shape of the isotherm, only increases its size, also increasing the HAZ. The dendrite arm spacing is strongly dependent on the cooling rate. Increasing the cooling rate causes smaller dendrite arm spacing.

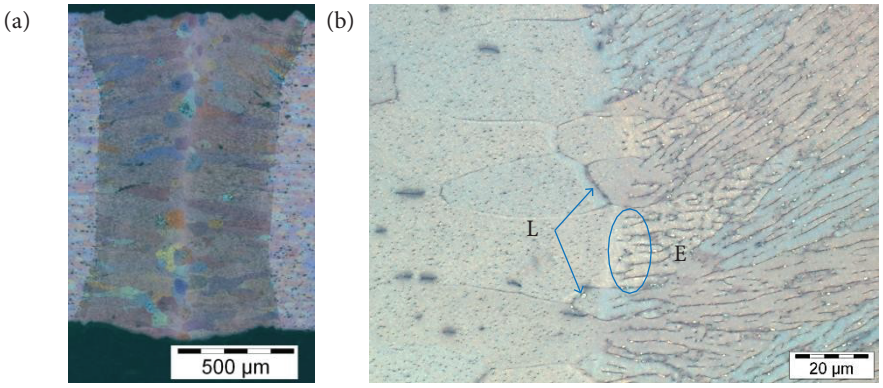

Figure 7. (a) Micrograph of the sample E cross section; and (b) region next to the fusion line of sample E, showing liquation (L) and epitaxial growth (E).

The cooling rate determines grain structure and formed phases, directly affecting the mechanical properties. Increasing the heat input causes a reduction in the cooling rate. On the other hand, increasing the speed also increases the cooling rate.

Figure 8 presents the measurements of the Vickers Hardness (HV) as a function of the distance from the centerline for the conditions A, D, E, and F. The other two conditions presented a central crack, rendering the measurements unviable. A sensible drop in HV can be seen in all conditions, from about 110 HV of the base material to a range between 75 and 95 HV.

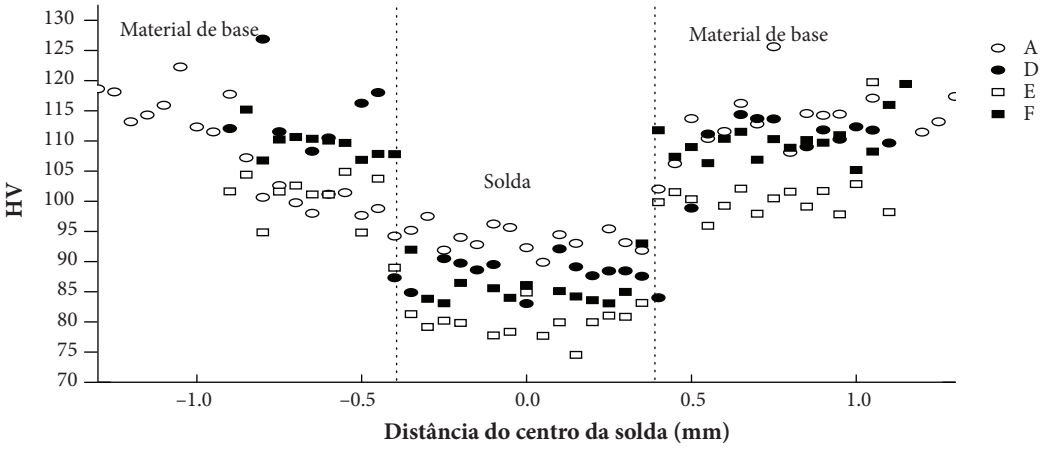

Figure 8. Vickers Hardness profile for the samples A, D, E, and F.

The wide variation of HV in the base material is due to the presence of sporadic precipitates. These precipitates disappeared after laser welding and were replaced by interdendritic microsegration, which is less effective in terms of hardening. Additionally, the indentator, Berkovich-type, has a nanometric tip and any variation of the material could lead to a wide scatting. The loss of hardness in the welded region could be considered a threat, particularly in mechanical applications, because of the tendency of striction.

MORPHOLOGY OF THE WELDS

Considering only the welds with full penetration and without defects, the conditions D and E are eligible for the morphological study. 3D models were generated through the roughness measurement of the upper and lower surfaces of the samples, as observed in Fig. 9. In the images, some differences in the solidification structure between samples D and E can be observed, both in the shape of the upper surface, with a "V" trail on the left and a "U" trail on the right, as well as on the surface finish of the lower surface. In the case of experiment E, dross was observed, red peaks of up to 300 μm, that can cause a lack of material inside the weld bead, causing tensile tensions, cracks, and porosity in these regions.

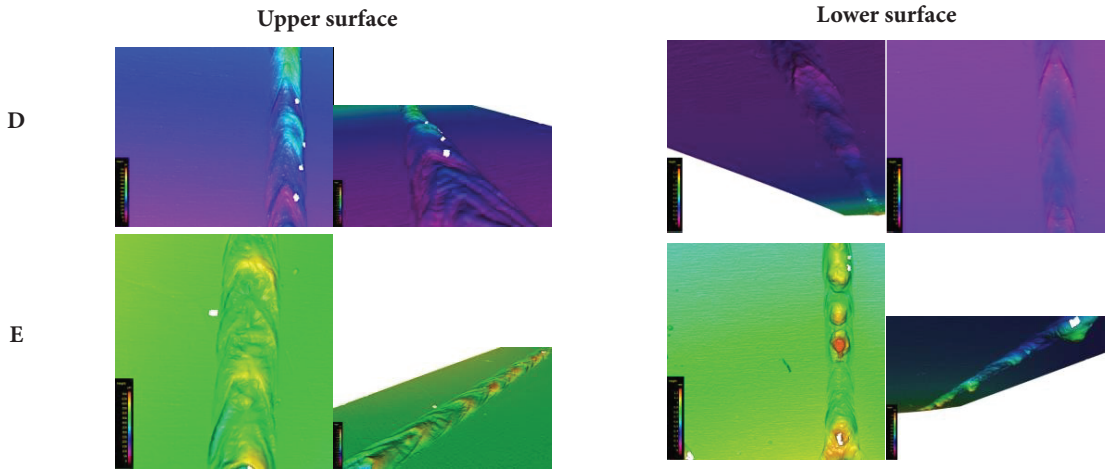

Figure 9. 3D surface rendering of the upper and lower surfaces for the samples D and E.

In the laser welding process it is common to observe solidification humps, which occur periodically throughout the process. These cyclically occurring humps can cause several problems by discontinuity in solidification. This effect is clearly visible in Figs. 9 and 10.

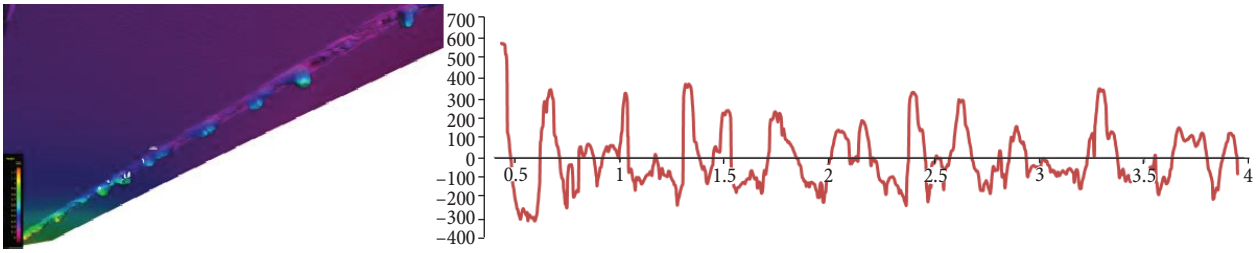

Figure 10. Dropouts in the lower surface of the weld bead – sample E. The axes are: vertical the height in micrometers, and horizontal the distance in millimeters.

In the upper surface of experiment D, small humps occurred with an average distance of 200 μm. For experiment E, they occurred approximately every 2.5 mm. It can also be noticed that periodic problems occurred every 2.5 mm on the lower surface of the same sample. When the welding speed is low, i.e., sample E in comparison to D, the molten Al had more time to flow to

the upper and lower regions of the weld. The dropout was due to the positive pressure of the keyhole and the lower flow can be associated to the metallostatic pressure and viscosity of the Al melt. Although clearly different in terms of liquid aluminum flow, both D and E conditions presented the same heat input and similar absorptivities, showing that processing speed plays an important role in the final shape of the weld bead.

CONCLUSIONS

The same heat input produced very different macrostructures and microstructures. In this study, a better understanding was sought about the influence of heat input in the processing of the welded aluminum alloy through a comparative study.

In the literature, many authors use the heat input as the reference source for the energy input provided during processing. While this practice is traditional and works reasonably well for the conventional welding methods, for the laser processing, and might be for some others, it may not be the most appropriate alternative. The heat input, which is widely used nowadays, does not take into account the real energy absorbed by the material, which can bring several implications on the processing and the expected results for a given supplied energy.

Considering Heat Input as the only main source of information on the amount of energy used during a laser material processing can cause a great divergence between the expected and the actual result. For example, in this study, two opposing processes (welding and cutting) were obtained with the same heat input. The real heat transfer from the laser keyhole of the material is dependent of the absorptivity. If the actual assumptions of the absorptivity are correct, its value changed from 4.6% to 10.5%, even under the same heat input value.

In the present study, two different heat input values were set in order to evaluate possible differences in the resulting macro and microstructure. For a heat input of 13 J/mm, in experiments D, E, and F, very different welding results were obtained, from acceptable welds to the appearance of solidification cracks and pores. A heat input of 30 J/mm resulted in two very different processes, welding (sample A), and cutting (samples B and C). This difference is simply due to the difference in the parameters to obtain the same heat input.

The presence of equiaxed or columnar grains also changed under the same heat input and is related to the cooling rate. The percentages of equiaxed grains were 13%, 21% and, 24% for speeds 50, 100, and 150 mm/s, respectively. Considering the thermal gradient at the weld centerline were 204.78, 257.51, and 483.87 °C/mm for D, E, and F, respectively, the current grain distribution corroborates the standard theory.

The major problems verified are the loss of precipitates in the weld bead, which decreases the local hardness, and the presence of weld humps and drop-out. These features were verified in the same heat input.

AUTHOR'S CONTRIBUTION

Conceptualization, Coelho BN and Carvalho SM; Methodology, Coelho BN; Investigation, Coelho BN; Lima MSF, Carvalho SM, and Costa, AR.; Writing – Original Draft, Lima MSF and Costa AR; Writing – Review and Editing, Costa AR and Carvalho SM; Supervision, Lima MSF.

REFERENCES

Braun R (2005) Laser beam welding of Al-Mg-Si-Cu alloy 6013 sheet using silicon rich aluminium filler powders. Materials Science and Technology 21(1):133-140. doi: 10.1179/174328405X16225

Enginneering Toolbox (2003) Latent heat of melting for some common materials. The Engineering Toolbox; [accessed 2017 June 20]. http://www.engineeringtoolbox.com/latent-heat-melting-solids-d_96.html

Higashi ALC, Lima MSF (2012) Occurrence of defects in laser beam welded Al-Cu-Li sheets with T-joint configuration. J Aerosp Technol Manag 4(4):421-429. doi: 10.5028/jatm.2012.04044212

Huntington CA, Eagar TW (1982) Laser welding of aluminum and aluminum alloys. Presented at: 63rd AWS Annual Convention. Welding Research Supplement; Kansas, USA.

Ion J (2005) Laser Processing of Engineering Materials. Amsterdam: Elsevier.

Kannatey-Asibu Jr. E (2009) Principles of Laser Materials Processing. New Jersey: John Wiley & Sons.

Kaplan A (1994) A model of deep penetration laser welding based on calculation of the keyhole profile. Journal of Physics D: Applied Physics 27(9):1805-1814. doi: 10.1088/0022-3727/27/9/002

Kurz W, Bezençon C, Gäumann M (2001) Columnar to equiaxed transition in solidification processing. Science and Technology of Advanced Materials 2(1):185-191. doi: 10.1016/S1468-6996(01)00047-X

Kurz W, Fisher DJ (1989) Fundamentals of solidification. 3rd ed. Aedermannsdorf: Trans Tech Publications.

Leigh BR, Poon C, Kerr HW, Lawson WHS, Ferguson NG (2002) An evaluation of the physical properties of Nd:YAG laser welded high strength 6000 series aluminum alloys. Presented at: ICAS 2002 Congress. Proceedings of the ICAS 2002 Congress; Toronto, Canada.

Lima MSF (2016) Phase transformations during laser processing of aerospace metallic materials. Advanced Materials Research 1135:179-201. doi: 10.4028/www.scientific.net/AMR.1135.179

MakeItFrom (2017) 6013 (AlMg1Si0.8CuMn, A96013) Aluminum. MakeItFrom.com; [accessed 2017 June 20]. http://www.makeitfrom.com/material-properties/6013-AlMg1Si0.8CuMn-A96013-Aluminum

Martorano MA, Beckermann C, Gandin C-A (2003) A solutal interaction mechanism for the columnar-to-equiaxed transition in alloy solidification. Metallurgical and Materials Transactions A 34(8):1657-1674. doi: 10.1007/s11661-003-0311-x

Mendez PF, Eagar TW (2001) Welding processes for aeronautics. Advanced Materials & Processes 159(5):39-43.

Passini A, Oliveira AC, Riva R, Travessa DN, Cardoso KR (2011) Ultrasonic Inspection of AA6013 Laser Welded Joints. Materials Research 14(3):417-422. doi: 10.1590/S1516-14392011005000057

Quintino L, Miranda R, Dilthey U, Iordachescu D, Banasik M, Stano S (2012) Laser welding of structural aluminium. In: Moreira P, Silva L, Castro P, editors. Structural Connections for Lightweight Metallic Structures. Advanced Structural Materials. v 8. Berlin: Springer-Verlag. doi: 10.1007/8611_2010_46

Riva R, Siqueira RHM, Lima MSF (2015) Crack-free autogeneous one-sided laser welding of a 6013 aluminum alloy T-joint for aircraft applications. Presented at: Lasers in Manufacturing Conference 2015. Proceedings of LIM 2015; Munich, Germany. Bochum: WLT.

Rosenthal D (1946) The theory of moving sources of heat and its application to metal treatments. Transactions of the A.S.M.E. 68:849-866.

Siqueira RHM, Riva R, Abdalla AJ, Lima MSF (2015) Mechanical and microstructural characterization of aluminium alloy AA 6013 submitted to different thermal treatments. Rev Bras Apl Vac 34(2):49-53. doi: 10.17563/rbav.v34i2.924

Sonti N (1988) Influence of process parameters on laser weld characteristics in aluminum alloys. (TR 88-011). Applied Research Laboratory Technical Report.

Steen WM, Mazumder J (2010) Laser material processing. 4th ed. London: Springer-Verlag. doi: 10.1007/978-1-84996-062-5

Tu JF, Paleocrassas AG (2010) Low speed laser welding of aluminium alloys using single-mode fiber lasers. In: Na X, editor. Laser Welding. London: InTechOpen. doi: 10.5772/9857

Tzou DY (1989) On the thermal shock wave induced by a moving heat source. Journal of Heat Transfer 111(2):232-238. doi: 10.1115/1.3250667

Wang CY, Beckermann C (1994) Prediction of columnar to equiaxed transition during diffusion-controlled dendritic alloy solidification. Metallurgical and Materials Transactions A 25(5):1081-1093. doi: 10.1007/BF02652282

Wang XJ, Lu FG, Wang HP, Cui HC, Tang XH, Wu YX (2015) Experimental and numerical analysis of solidification cracking behaviour in fibre laser welding of 6013 aluminium alloy. Science and Technology of Welding and Joining 20(1):58-67. doi: 10.1179/1362171814Y.0000000254